CrossMark

Small-Scale Mechanical Testing on Proton Beam-Irradiated 304 SS from Room Temperature to Reactor Operation Temperature

H. VO [iD],[1,4] A. REICHARDT,[1] C. HOWARD,[1] M. D. ABAD,[1] D. KAOUMI,[2] P. CHOU,[3] and P. HOSEMANN[1,5]

1.—Department of Nuclear Engineering, UC Berkeley, Berkeley, CA, USA. 2.—Mechanical Engineering Department, University of South Carolina, Columbia, SC 29208, USA. 3.—Electric Power Research Institute, Palo Alto, CA, USA. 4.—e-mail: sfhivo@berkeley.edu. 5.—e-mail: peterh@berkeley.edu

Austenitic stainless steels are common structural components in light water reactors. Because reactor components are subjected to harsh conditions such as high operating temperatures and neutron radiation, they can undergo irradiation-induced embrittlement and related failure, which compromises reliable operation. Small-scale mechanical testing has seen widespread use as a testing method for both ion- and reactor-irradiated materials because it allows access to the mechanical properties of the ion beam-irradiated region, and for safe handling of a small amount of activated material. In this study, nanoindentation and microcompression testing were performed on unirradiated and 10 dpa proton-irradiated 304 SS, from 25°C to 300°C. Increases in yield stress (YS), critical resolved shear stress (CRSS) and hardness (H) were seen in the irradiated region relative to the unirradiated region. Relationships between H, YS, and CRSS of irradiated and unirradiated materials are discussed over this temperature range.

INTRODUCTION

The degradation of mechanical properties of materials in nuclear environments is a major issue in the nuclear industry. Understanding material performance and the failure mechanisms of reactor components in reactor environments remains critical. Testing reactor-irradiated materials poses constraints due to lengthy time scales and material activation. Ion beam irradiation is a surrogate irradiation technique, allowing accelerated materials evaluation under reactor-relevant conditions with full control of irradiation parameters and little to no activation if the ion beam energy is below material-specific thresholds.[1–3]

Since the ion beam irradiation depth is typically limited to tens of micrometers, small-scale mechanical testing (SSMT) is most suitable. Nanoindentation, microcompression, and other SSMTs have been studied.[4–8] Nanoindentation evaluates local hardness changes in the irradiated area with minimal sample preparation. Elevated temperature nanoindentation measurement capabilities have developed considerably[9,10] to evaluate the hardness (H) and reduced modulus (E_r) of many materials,[10,11] and to study deformation mechanisms at different temperatures.[11–13] It is challenging to extract macroscopic mechanical properties like yield stress (YS) from nanoindentation because of non-uniaxial stress states.[4] Microcompression testing complements nanoindentation by providing more accurate estimates of YS and other parameters.[8]

Little data exist on both nanoindentation and microcompression at elevated temperatures on the same irradiated material. Due to differences in deformation mechanisms which occur at increased temperatures, evaluating materials properties at reactor operation temperatures is important to assess in-service conditions. Here, nanoindentation and microcompression are expanded to elevated temperatures to assess material performance at both room temperature (RT) and reactor operation conditions.

EXPERIMENTAL PROCEDURES

Sample Irradiation

The 304 SS has a nominal wt.% composition of 18–20% Cr, 8–12% Ni, <2% Mn and <0.03% C. Before irradiation, the incident surface was
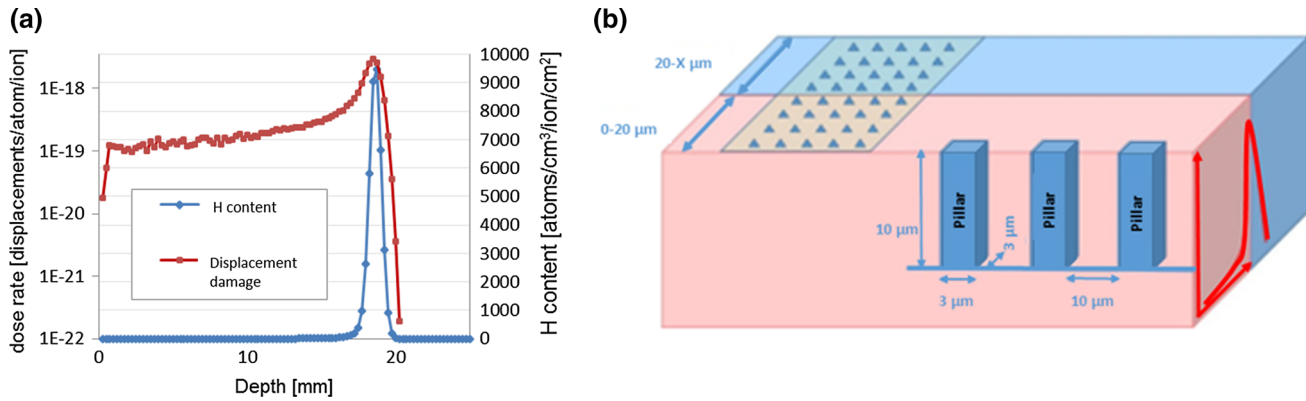
(a)

(b)

Fig. 1. (a) SRIM plot of dose profile. (b) Sketch of the sample. The red region represents the irradiation damage. A schematic plot of the dose profile is drawn on the side, where the maximum dose peak is 20 μm from the sample edge.

mechanically polished and electropolished to provide a suitable surface for irradiation. Samples were irradiated using 2 MeV protons to a dose of 10 dpa at $360 \pm 10°C$ in a Tandetron accelerator at the Michigan Ion Beam Laboratory. Based on SRIM calculations, the dose rate is $\sim8 \times 10^{-6}$ dpa/s assuming full cascade with a displacement energy of 40 eV.[14] The irradiation temperature approximates light water reactor operating temperatures plus the temperature shift accounting for the accelerated irradiations.[3] A description of the proton irradiation procedures is presented in Ref. [15]. Figure [1]a shows the dose profile with the ion penetration depth of approximately 20 μm based on SRIM calculations.

Pillar Fabrication

A FEI Quanta 3D FEG dual beam, with a focused Gallium-69$^+$ ion beam and a SEM, was utilized. Pillar manufacturing is described in Ref. [16]. Pillar dimensions were ~3 μm $\times$ ~3 μm $\times$ ~10 μm. Figure [1]b shows a schematic of the testing configuration. Electron backscattered diffraction (EBSD) was used to map grains close to the sample's irradiated edge and in the unirradiated region to identify single-grain testing regions. Tests of the same temperature were performed on pillars located in the same grain to make a direct comparison. The pillars were fabricated in the flat part of the dose curve not targeting the transition between the irradiated and unirradiated zone.

High Temperature Nanoindentation and Microcompression

Nanoindentation and ex situ microcompression experiments, seen in Fig. [1]b, at high temperature were conducted using the Micro Materials NanoTest^{TM} center. The indenter was placed in a purge chamber during heating with pure argon to keep the oxygen level below 2%. Measurements were conducted at 25°C, 50°C, 100°C, 200°C and 300°C. Mounting to the hot stage was done using ceramic paste (OMEGATHERM$^®$). The bond was cured for 24 h before testing. Nanoindentation measurements with a cubic boron nitride (cBN) Berkovich indenter were performed in cross-section with respect to the irradiated surface. cBN is a suitable material for these tests whereas diamond disintegrates at elevated temperatures.[17] Indents, placed 5 μm apart to avoid plastic zone overlap, were introduced in a depth-controlled mode up to 300 nm at a 1 mN/s loading rate, a 2 mN/s unloading rate, and a 30 s dwell time. 50 indent arrays were performed on areas containing both non-irradiated and irradiated regions, shown in Fig. [1]b. The thermal drift was below 0.3 nm/s. The last 60% of the 70-s drift measurement at the end of each unloading cycle at 10% of the maximum peak load was used. Hardness and E_r were calculated using load–displacement curves by the Oliver–Pharr method.[18] The location of the indents was measured in the SEM.

For microcompression, a flat punch 10-μm-diameter diamond indenter was used. For proper alignment, test indents were made on the surface to verify the alignment as in Refs. [19], [20]. The indenter was used to measure the misalignment angle of the sample by contacting the sample surface at several points. Slopes in the x and y directions were recorded and the tilt was corrected accordingly. Fine alignment was conducted by evaluating the shape of the imprint of the flat punch. A 100-nm-deep imprint with a 10-μm flat punch leads to a maximum misalignment angle of 0.57°.

After alignment, the pillars were compressed using the load controlled mode. Loading rates were 0.02–0.05 mN/s and unloading rates ~0.01 mN/s. The tests were stopped manually after yielding. The waiting time before each test to achieve thermal stability of the indenter tip and the specimen was 10 min. A total of 30–40 compression tests were performed in non-irradiated and irradiated single grain regions. Due to the large number of pillars and the limited grain size, not all pillars were fabricated in the same grain. EBSD verified the individual grain orientation. About 15 pillars were used for alignment technique development process, while 2–5 pillars were tested at each temperature for each dose condition.
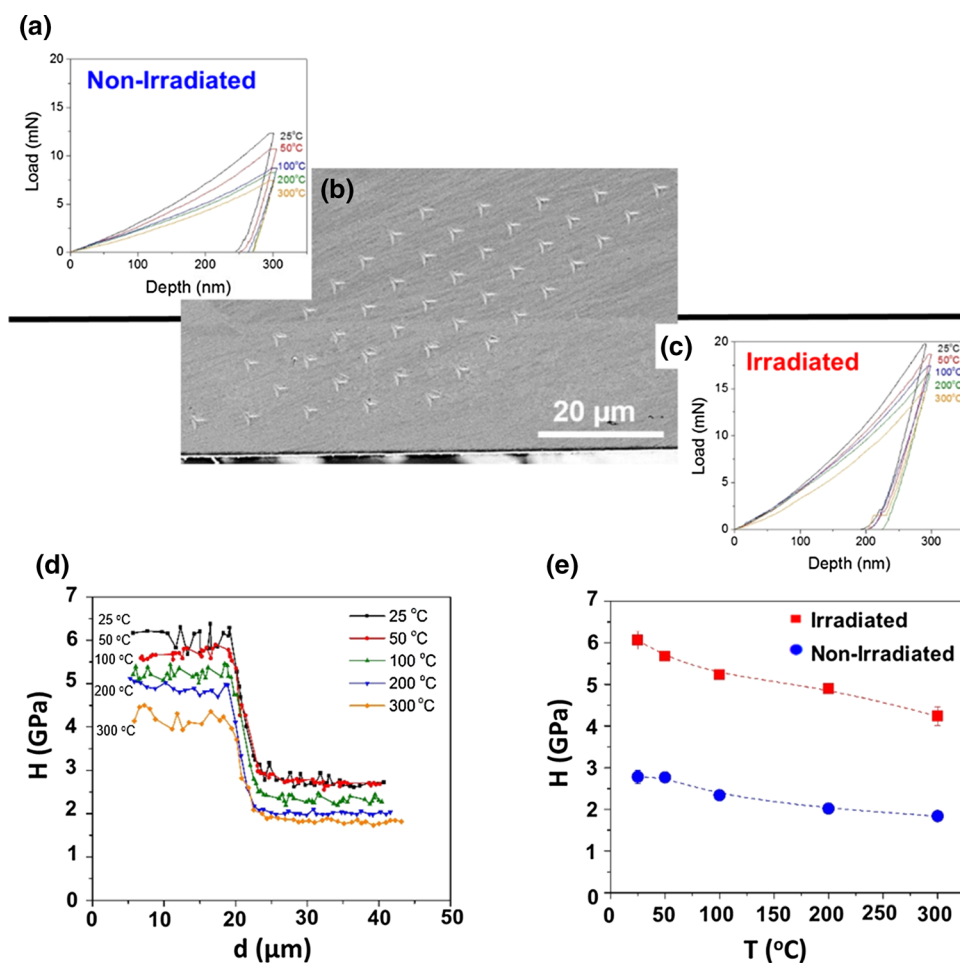
Fig. 2. Nanoindentation properties of irradiated and non-irradiated 304 SS between RT and 300°C. (a) Non-irradiated and (c) irradiated load–displacement measurements. (b) SEM micrograph of a representative array of nanoindents. (d) Hardness versus depth curves at various temperatures for indents in the irradiated region. (e) Hardness as a function of temperature for both irradiated and non-irradiated indents.

RESULTS

Nanoindentation

Representative load–displacement curves are shown in Fig. 2a and c. Hardness at different temperatures was calculated from curves obtained from the irradiated and non-irradiated regions seen in Fig. 1b. Since the location of each individual indent was measured using a SEM, all hardness data can be summarized in Fig. 2d as a function of the distance from the sample edge. Hardness measurements are approximately constant in the irradiated region, meaning irradiation hardening has saturated by the 10-dpa dose; they also confirm that the irradiation stopping point is ~20 μm from the sample surface. The hardness drops to the unirradiated bulk value after 20 μm. From Fig. 2e, the average hardness values of irradiated and non-irradiated materials are ~6 GPa and ~2.8 GPa at RT, but at 300°C they decrease to ~4.3 GPa and ~1.8 GPa. Differences in hardness between irradiated and non-irradiated regions decrease with increasing temperature.

Microcompression

Microcompression tests were performed up to 300°C in irradiated and non-irradiated areas. There was insignificant change in YS with respect to temperature for non-irradiated tests, whereas the YS for irradiated tests decreases significantly with respect to temperature, seen in Fig. 3d. At all testing temperatures, irradiated pillars are much stronger than their non-irradiated counterparts, seen in Fig. 3a, d and e.

Representative true stress–true strain curves calculated from the load–displacement curves are shown in Fig. 3a. When a pillar is compressed by the circular flat punch, the material below the pillar also slightly deforms. The bulk displacement must be accounted for in stress and strain calculations.[21,22] True stress–true strain curves were calculated using:[22]

$$\sigma(\text{MPa}) = \frac{\pi 10^{-12} F}{4A} \left(1 + \frac{10^{-9} d - \frac{1-\nu^2}{E\sqrt{\frac{4A}{\pi}}} 10^{-6} F}{h} \right) \quad (1)$$
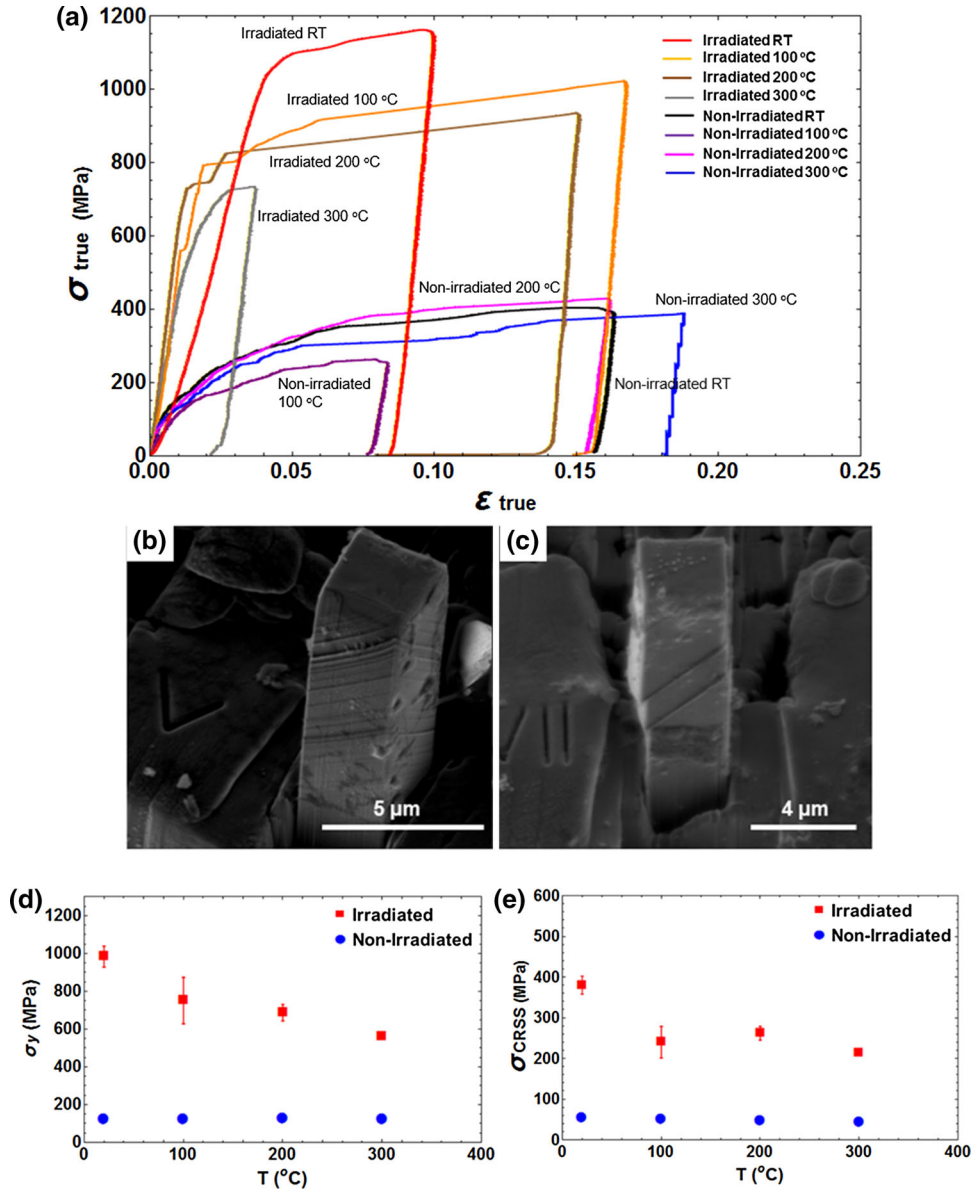
Fig. 3. Microcompression properties of irradiated and non-irradiated 304 SS between RT and 300°C. (a) Representative stress–strain curves for both non-irradiated and irradiated pillars spanning the range of temperatures tested. SEM images of a representative compressed, (b) non-irradiated pillar and (c) irradiated pillar at 100°C. (d) YS and (e) CRSS versus temperature.

$$\varepsilon = \ln\left(1 + \frac{10^{-9}d - \frac{1-v^2}{E\sqrt{\frac{4A}{\pi}}}10^{-6}F}{h}\right) \qquad (2)$$

where d (nm) is the recorded displacement, A (m²) is cross-sectional pillar area, E (Pa) is Young's Modulus, h (m) is pillar height and F (μN) is the recorded load.

Values of 0.2% YS were obtained from true stress–true strain plots by applying linear regression to the elastic region and finding the intersection between the curve and the regression line which is offset by 0.2% strain. Pillars with different grain orientations have different YS. Critical resolved shear stress (CRSS), the shear component

of the YS required to initiate plastic deformation, is calculated to account for the differences in crystal orientation by Schmidt's law:

$$\sigma_{\mathrm{CRSS}} = \sigma_y \cos(\varphi)\cos(\lambda) \qquad (3)$$

where φ is the angle between the normal of the slip plane and the direction of the applied force and λ is the angle between the slip direction and the direction of the applied force. σ_y is YS. φ and λ are determined from EBSD. The orientations are measured by EBSD on the surface of pillar tops, and it is assumed the single grain region extends to the base of the pillars. Post-test SEM images of the pillars can be seen in Fig. 3b and c. Pillars show multiple
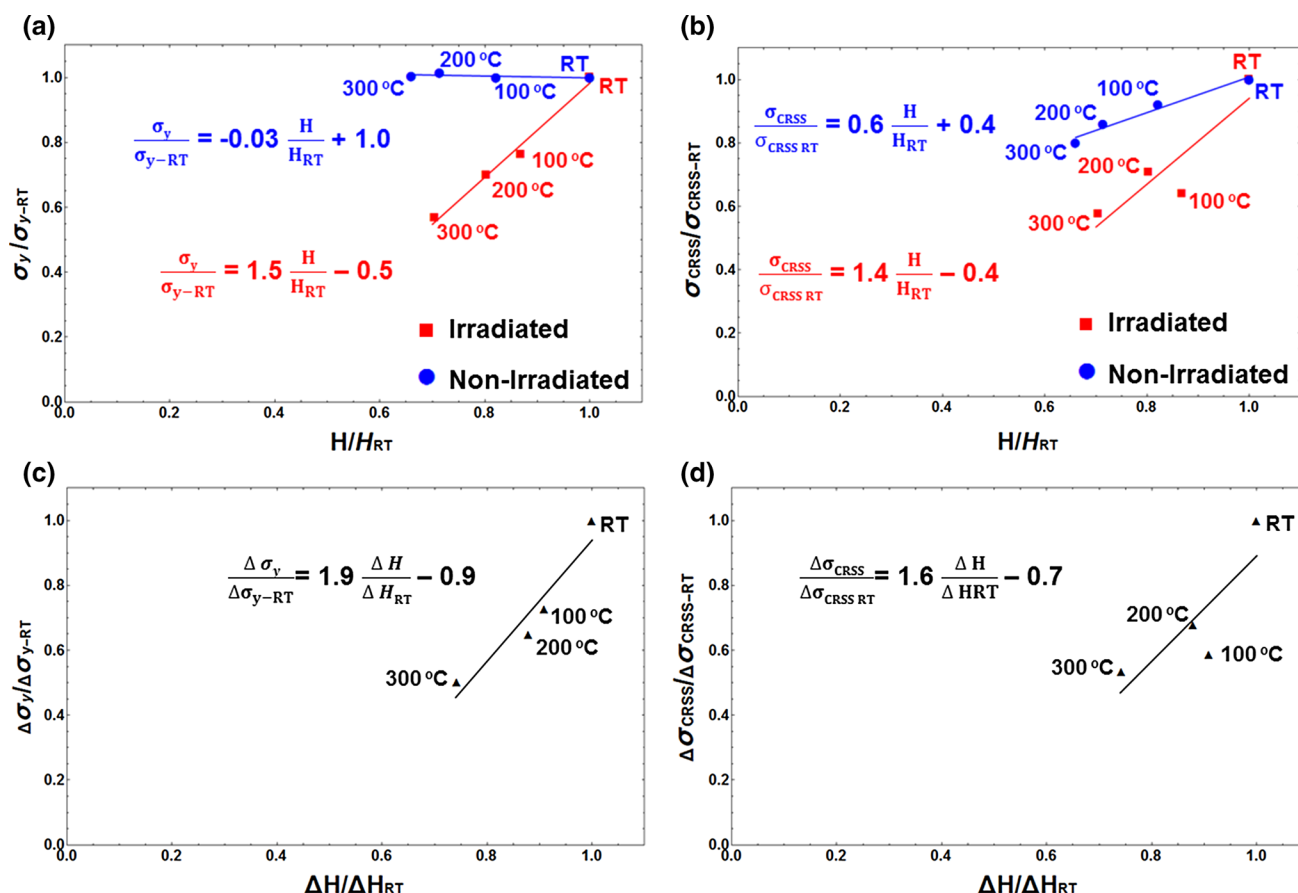
Fig. 4. Mechanical properties relationships of irradiated and non-irradiated 304SS normalized with respect to RT, with associated linear regression relationships. (a) YS versus hardness; (b) CRSS versus hardness; (c) ΔYS versus ΔH; and (d) ΔCRSS versus ΔH.

slip steps along the same planes for a given crystal orientation, which are assumed to be the maximum Schmid factor of that orientation.

YS and CRSS are shown in Fig. 3c and d. At all temperatures, YS and hardness values of irradiated regions are significant higher than non-irradiated values. The average YS of unirradiated and irradiated pillars at RT are ~127.5 MPa and ~984 MPa, respectively. The YS and CRSS of irradiated pillars decrease dramatically with increasing temperature. Since tests were conducted in different grains CRSS should be compared rather than YS. The YS of unirradiated 304SS does not vary significantly from RT to 300°C.[23] Non-irradiated pillars show more slip bands after deformation at all temperatures. Figure 3b and c, after the 100°C tests, shows that.

DISCUSSION

Figure 3b and c shows that irradiated material contains fewer but stronger slip events than unirradiated material. It is speculated that radiation damage pins dislocations and increases YS. However, once dislocations start moving, presumably defect-free channels can form which localize deformation. This formation of defect-free channels in combination with the higher energy stored in the

material (higher YS of irradiated material vs. unirradiated material) leads to sudden large slip steps as observed in SEM images at all temperatures.

Strength versus hardness relationships were determined using the pillar-measured YS and CRSS values from microcompression testing and compared against the nanoindentation data. Figure 4a shows average YS values normalized with respect to the YS at RT plotted against average hardness values normalized with respect to the hardness at RT for both non-irradiated and irradiated materials. A plot of average CRSS values against hardness values with the same normalization for both non-irradiated and irradiated materials is shown in Fig. 4b. Good linear correlations are presented for both irradiated and non-irradiated material. While the correlation in the unirradiated material shows nearly no change in YS, a significant change can be seen in CRSS. From RT to 300°C, the relationship for irradiated and unirradiated materials can be described with the equations in Fig. 4a and b. Tensile testing over the same temperature range has been conducted on 304SS (not the same heat). It was found that the correlation especially with the YS converted from the hardness data as described in Ref. 24 is very good and the macroscopic YS of

267 MPa (RT), 201 MPa (100°C) and 162 MPa (300°C) can be found. This correlates well with YS numbers converted from hardness data, as described in Ref. 25, of 282 MPa (RT), 208 MPa (100°C) and 126 MPa (300°C) while the pillar data of 127 MPa, 127 MPa and 126 MPa (RT, 100°C and 300°C, respectively) does not follow quite as well but is in the same regime due to the fact that different crystal orientations were measured in the pillar experiment. Without further TEM, no detailed explanations can be given and one can only speculate about the detailed mechanism. However, this indicated that the properties at reactor operation temperature must be measured directly and cannot easily be determined by estimations from RT data. Figure 4c and d displays the relationships between the changes from an unirradiated property to an irradiated property over the different temperatures. While similar comparisons were made in the past for different materials, leading to a number of empirical equations describing the relationship between hardness and YS at particular temperatures, these relationships have not been established over a range of temperatures. They are valuable for estimating materials' YS based on hardness testing at a given temperature.[26,27]

CONCLUSION

This study presents the development of an ex situ microcompression technique for characterizing proton-beam-irradiated materials at reactor operating temperatures. Micro-pillars have been prepared from irradiated and non-irradiated 304SS and compressed over a range of temperatures from RT to 300°C. The hardness and YS of irradiated materials are significantly greater than non-irradiated materials, with the irradiated region decreasing more dramatically than the non-irradiated region with respect to increasing temperature. Irradiated pillars deform through fewer slip bands than non-irradiated pillars at all temperatures.

ACKNOWLEDGEMENTS

REFERENCES

1. G.S. Was, *Trans. Am. Nucl. Soc.* 98, 1023 (2008).
2. F.U. Naab, E.A. West, O.F. Toader, and G.S. Was, *AIP Conf. Proc.* 1336, 325 (2011).
3. G.S. Was, J.T. Busby, T. Allen, E.A. Kenik, A. Jensson, S.M. Bruemmer, J. Gan, A.D. Edwards, P.M. Scott, and P.L. Andreson, *J. Nucl. Mater.* 300, 198 (2002).
4. P. Hosemann, D. Kiener, Y. Wang, and S.A. Maloy, *J. Nucl. Mater.* 425, 136 (2012).
5. P. Hosemann, J.G. Swadener, D. Kiener, G.S. Was, S.A. Maloy, and N. Li, *J. Nucl. Mater.* 375, 135 (2008).
6. D. Kiener, A.M. Minor, O. Anderoglu, Y.Q. Wang, S.A. Maloy, and P. Hosemann, *J. Mater. Res.* 27, 2724 (2012).
7. J.P. Ligda, Q. Wei, W.N. Sharpe, and B.E. Schuster, *Dynamic Behavior of Materials*, 2014th ed. (New York: Springer, 2013), p. 427.
8. D. Kiener, W. Grosinger, G. Dehm, and R. Pippan, *Acta Mater.* 56, 580 (2008).
9. J.M. Wheeler, D.E.J. Armstrong, W. Heinz, and R. Schwaiger, *Curr. Opin. Solid State Mater. Sci.* 2015.
10. M.R. de Figueiredo, M.D. Abad, A.J. Harris, C. Mitterer, and P. Hosemann, *Thin Solid Films* 578, 20 (2015).
11. J.M. Wheeler, V. Maier, K. Durst, M. Goken, and J. Michler, *Mater. Sci. Eng. A* 585, 108 (2013).
12. M. Kreuzeder, M.D. Abad, M.-M. Primorac, P. Hosemann, V. Maier, and D. Kiener, *J. Mater. Sci.* 50, 634 (2014).
13. M.-M. Primorac, M.D. Abad, P. Hosemann, M. Kreuzeder, V. Maier, and D. Kiener, *Mater. Sci. Eng. A* 625, 296 (2015).
14. J.F. Ziegler and J.P. Biersack, *SRIM Program* (Yorktown, NY: IBM Corp., 2008).
15. G. Gupta, Z. Jiao, A.N. Ham, J.T. Busby, and G.S. Was, *J. Nucl. Mater.* 351, 162 (2006).
16. D. Kiener, C. Motz, T. Schöberl, M. Jenko, and G. Dehm, *Adv. Eng. Mater.* 8, 1119 (2006).
17. J.M. Wheeler, R.A. Oliver, and T.W. Clyne, *Diam. Relat. Mater.* 19, 1348 (2010).
18. W.C. Oliver and G.M. Pharr, *J. Mater. Res.* 7, 1564 (1992).
19. C. Shin, S. Lim, H. Jin, and P. Hosemann, *J. Kwon J. Nucl. Mater.* 444, 43 (2014).
20. M.D. Uchic and D.M. Dimiduk, *Mater. Sci. Eng. A* 400–401, 268 (2005).
21. H. Wörgötter, D. Kiener, J.M. Purswani, D. Gall, and G. Dehm, *BHM Berg. Hüttenmänn. Monatshefte* 153, 257 (2008).
22. I. Sneddon, *Int. J. Eng. Sci.* 3, 47 (1965).
23. 304/304L Stainless Steel Production Data Bulletin (AK Steel Corporation 2013). http://www.aksteel.com/pdf/markets_products/stainless/austenitic/304_304l_data_bulletin.pdf. Accessed 12 May 2015.
24. A. Lupinacci, K. Chen, Y. Li, M. Kunz, Z. Jiao, G.S. Was, M.D. Abad, A.M. Minor, and P. Hosemann, *J. Nucl. Mater.* 458, 70 (2015).
25. P. Hosemann, A. Reichard, A. Lupinacci, C. Howard, H. Vo, M.D. Abad, D. Kaoumi, and P. Chou, *Proceedings of the 17th International Conference on Environmental Degradation of Materials in Nuclear Power Systems—Water Reactors* (2015).
26. J. Outinen and P. Makelainen, *Fire Mater.* 28, 237 (2004).
27. D.J. Edwards, A. Schemer-Kohrn, and S. Bruemmer, *Characterization of Neutron-Irradiated 300-Series Stainless Steels* (Palo Alto, CA: EPRI, 2006).